



Guadalupe, T., Mathias, S. R., vanErp, T. G. M., Whelan, C. D., Zwiers, M. P., Abe, Y., Abramovic, L., Agartz, I., Andreassen, O. A., Arias-Vásquez, A., Aribisala, B. S., Armstrong, N. J., Arolt, V., Artiges, E., Ayesa-Arriola, R., Baboyan, V. G., Banaschewski, T., Bastin, M. E., Baune, B. T., ... Francks, C. (2017). Human subcortical brain asymmetries in 15,847 people worldwide reveal effects of age and sex. *Brain Imaging and Behavior*, 11(5), 1497-1514.  
<https://doi.org/10.1007/s11682-016-9629-z>

Publisher's PDF, also known as Version of record

License (if available):  
CC BY

Link to published version (if available):  
[10.1007/s11682-016-9629-z](https://doi.org/10.1007/s11682-016-9629-z)

[Link to publication record in Explore Bristol Research](#)  
PDF-document

This is the final published version of the article (version of record). It first appeared online via Springer at <https://link.springer.com/article/10.1007%2Fs11682-016-9629-z>. Please refer to any applicable terms of use of the publisher.

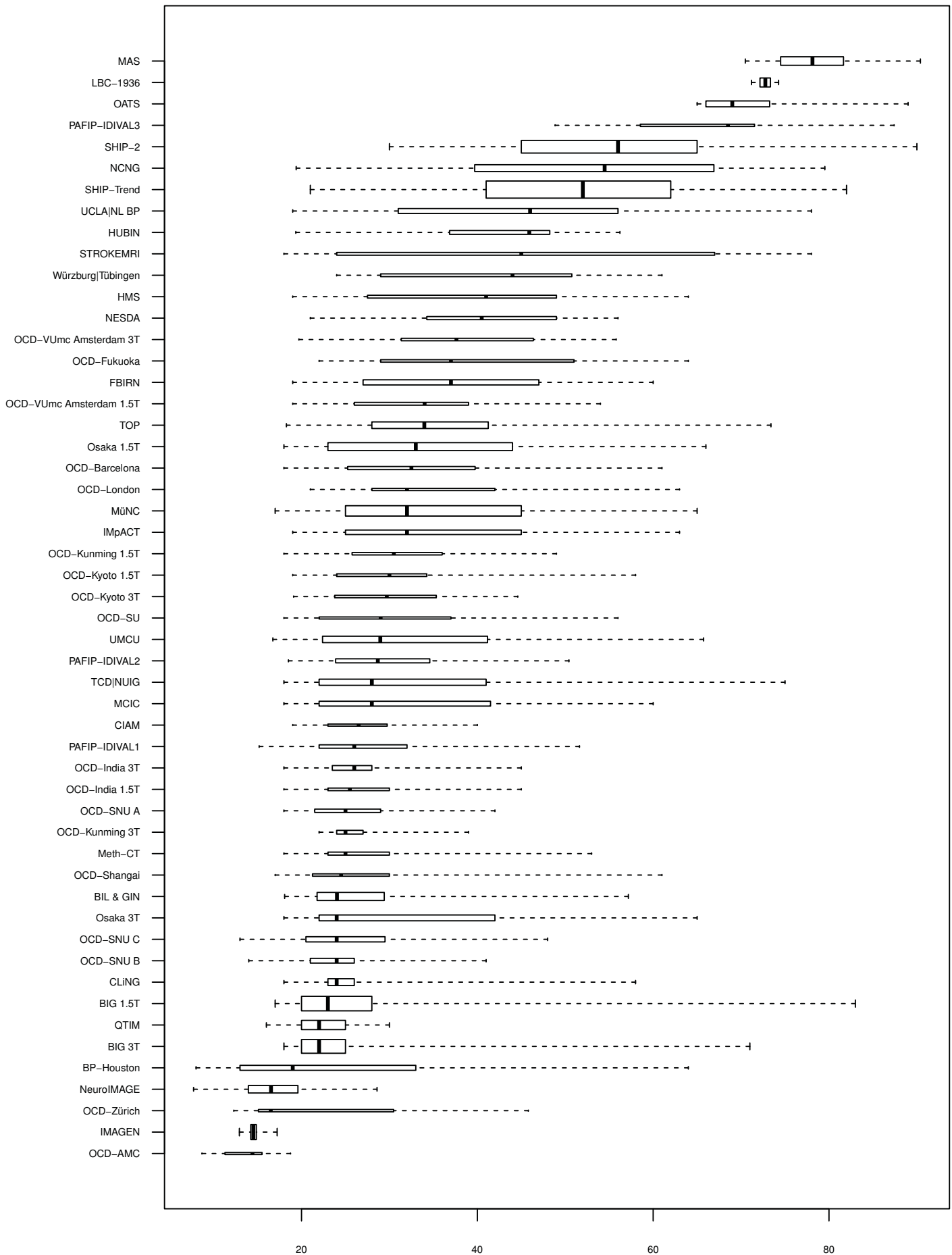
## University of Bristol - Explore Bristol Research

### General rights

This document is made available in accordance with publisher policies. Please cite only the published version using the reference above. Full terms of use are available:  
<http://www.bristol.ac.uk/pure/user-guides/explore-bristol-research/ebr-terms/>

Supporting Information S1. Boxplots show the age distributions per cohort. The datasets are ordered vertically by median age, oldest at the top. On the  $x$ -axis are the age values (in years). The horizontal length of each box represents the age at the 2nd and 3rd quartile of their distribution (thus containing half the respective dataset). The vertical width of the boxes is proportional to the square root of the dataset sample size. Boxes are split at the median age, and the whiskers reach to the minimum and maximum ages.

# Age distributions per dataset





Supplemental Information S3. List of datasets (arranged alphabetically) on which handedness analyses were performed, corresponding sample sizes and assessment methods.

Dataset	Left handed	Right handed	Assessment
BIG 1.5T	67	1205	Self-report
BIG 3T	56	1150	Self-report
BIL & GIN	205	248	Self-report
CLiNG	15	307	Self report confirmed by Edinburgh Handedness Inventory
FBIRN	5	173	Self-report
HMS	7	44	Self report confirmed by Edinburgh Handedness Inventory
HUBIN	6	90	Self-report
IMAGEN	160	1391	Self report confirmed by Purdue Pegboard test
IMpACT	15	126	Self-report
LBC-1936	34	522	Writing hand
MCIC	9	154	Annett Scale of Hand Preference
MüNC	14	729	Edinburgh Handedness Inventory: A threshold of 12 (out of 14) items was used to categorize as left- or right-handed.
NCNG	26	301	Self-report
NESDA	5	61	Self-report
NeuroIMAGE	45	333	Self-report
OCD-VUmc Amsterdam 1.5T	6	48	Self-report
OCD-VUmc Amsterdam 3T	7	31	Self-report
Osaka 1.5T	28	409	Self report confirmed by Edinburgh Handedness Inventory
Osaka 3T	11	226	Self report confirmed by Edinburgh Handedness Inventory
SHIP-2	57	1053	Self-report
SHIP-Trend	97	1943	Self-report
STROKEMRI	6	46	Self-report
TOP	22	279	Self-report
UCLA NL BP	20	140	Self-report
UMCU	36	227	Self-report

## Supplemental Information S4 : Left-right flip checks

Of special importance was to assure the correct correspondence between the left/right orientation of the processed image data and the original subject space. In contrast to the other axes (antero-posterior or superior-inferior), the correct orientation on the left-right axis is not directly identifiable from visual features, making it difficult to readily detect any erroneous image flips during processing. Such problems are much more unlikely since the adoption of the nifti imaging standard (<http://nifti.nimh.nih.gov/>), but they can still be a potential source of artifact if the raw (often DICOM-formatted) data is processed with incorrect assumptions (SPM documentation, p. 157; <http://www.fil.ion.ucl.ac.uk/spm/doc/manual.pdf>).

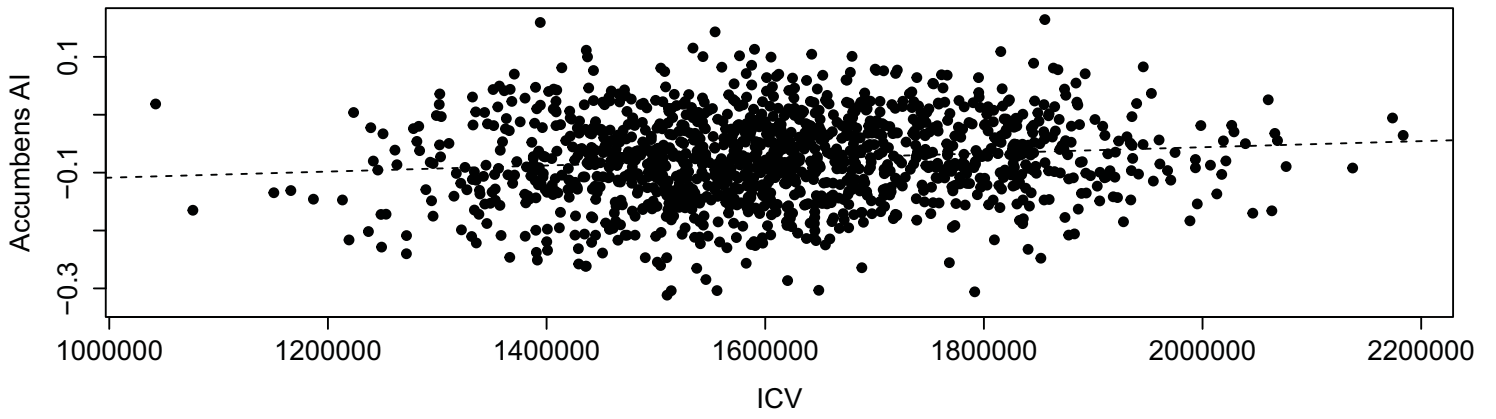
Because the ENIGMA protocol starts after the raw (often DICOM-formatted) data has been converted into an imaging standard (or converted by FreeSurfer itself), this meant that conversion from the DICOM format was the most likely step where any error could have taken place. This was assessed using several strategies, depending on the available information at each site. The **BIL & GIN**, **FBIRN**, **MAS**, **NESDA** and **OATS** samples had made use of paramagnetic fiducial markers on a subset of their subjects, thus eliminating orientation ambiguity. In **QTIM** and **SHIP**, subjects with a known unilateral brain abnormality were used to check the correct orientation of the image after conversion. In **BIG**, **CLING**, **HMS** and **OCD-SU**, a few examples were manually checked for mismatches between the DICOM and nifti header information, i.e. a correct flip from 'radiological' to 'neurological' orientation. Finally, we checked the consistency between several, commonly used, DICOM to nifti conversion tools and DICOM images generated from different manufacturers/models (using examples downloaded from the manufacturer's websites). The convertors used in this step were: "mri\_convert" ([https://surfer.nmr.mgh.harvard.edu/pub/docs/html/mri\\_convert.help.xml.html](https://surfer.nmr.mgh.harvard.edu/pub/docs/html/mri_convert.help.xml.html)), "MRIConvert" (<http://lcn.uoregon.edu/downloads/mriconvert>), "dcm2nii" (<http://www.cabiatl.com/mricro/mricron/dcm2nii.html>) and "spm\_dicom\_convert" (<http://www.fil.ion.ucl.ac.uk/spm/>).

Given that these checks yielded no problems, and that the datasets where no error was detected comprised 60% of the total meta-analysis sample, we were confident that such orientation errors must have been very unlikely.

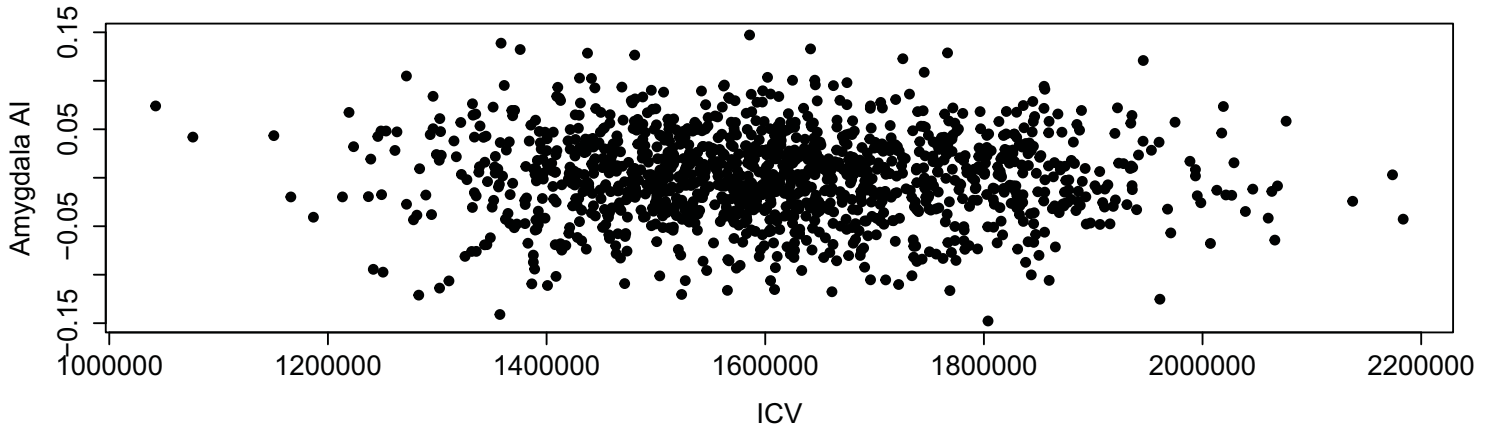
### **Supplementary Information S5.**

Plots of the relationship between ICV and subcortical AIs in the BIG 3T sample. Regression analyses of linear and quadratic relationships revealed only linear effects of ICV with AIs of the nucleus accumbens, caudate nucleus and putamen (as indicated by the dashed lines).

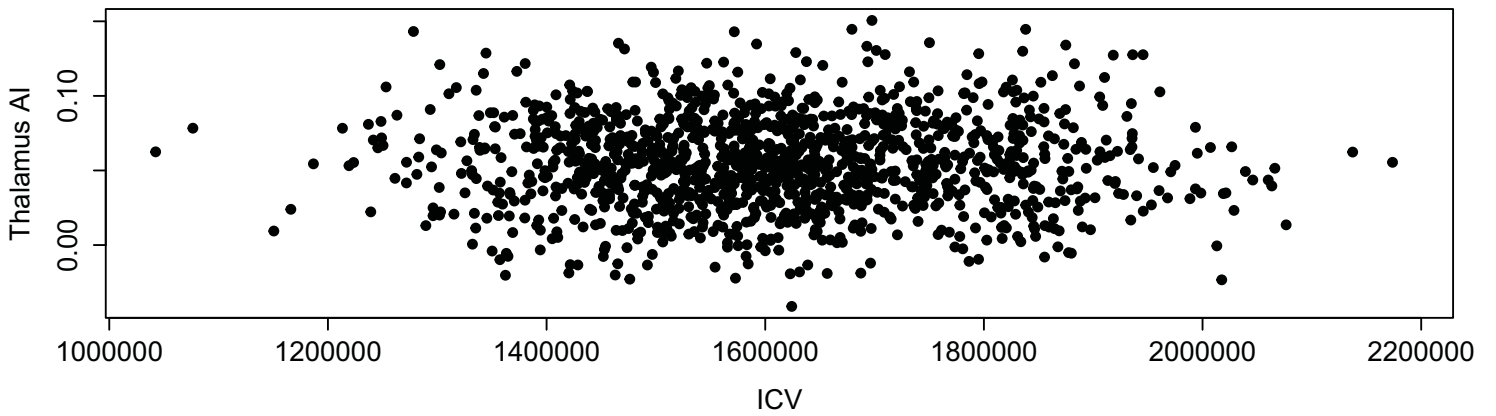
**N. accumbens AI against ICV**



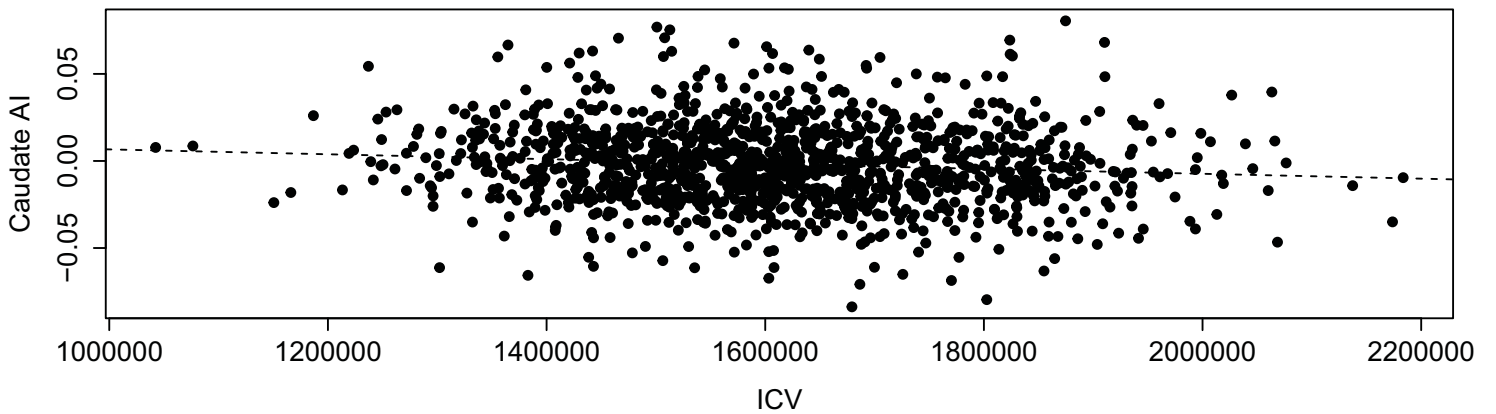
**Amygdala AI against ICV**



**Thalamus AI against ICV**

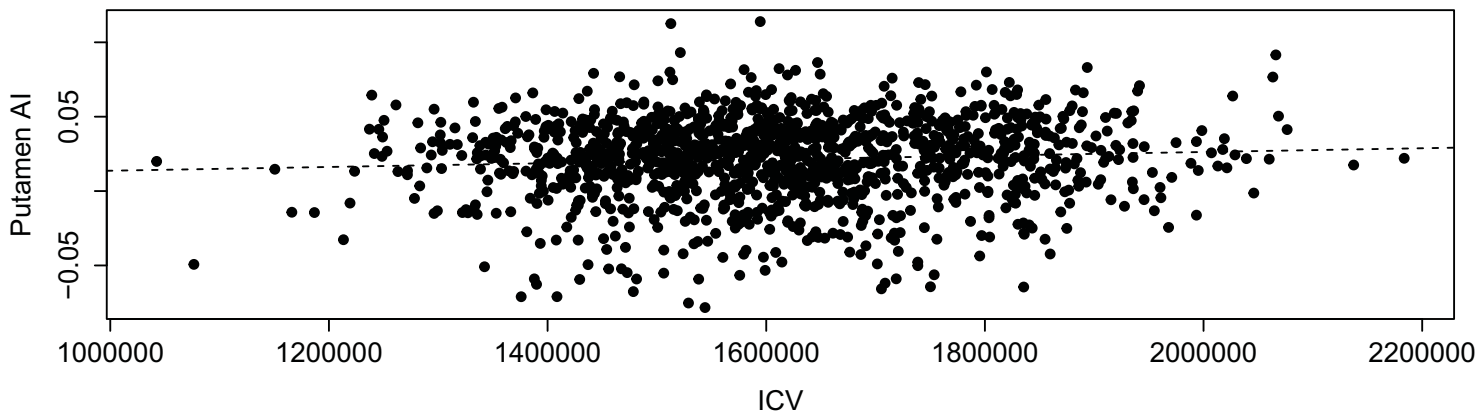


**Caudate N. AI against ICV**

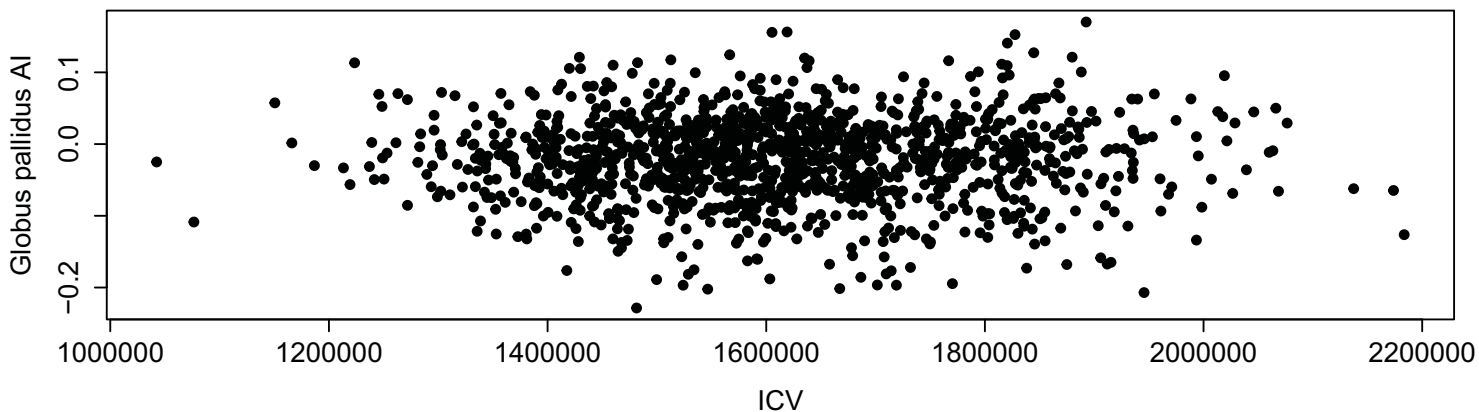




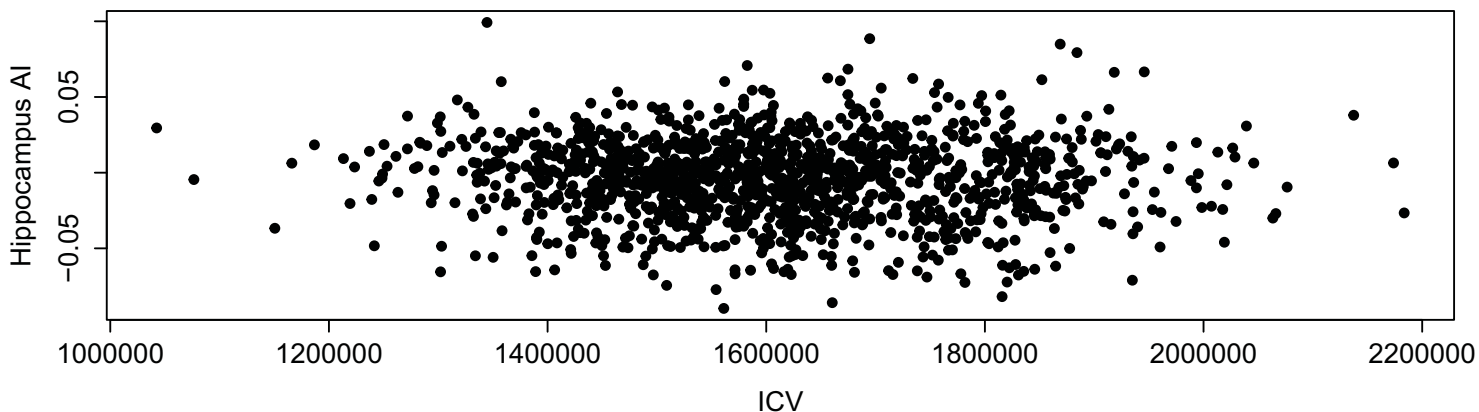
**Putamen AI against ICV**



**Globus Pallidus AI against ICV**



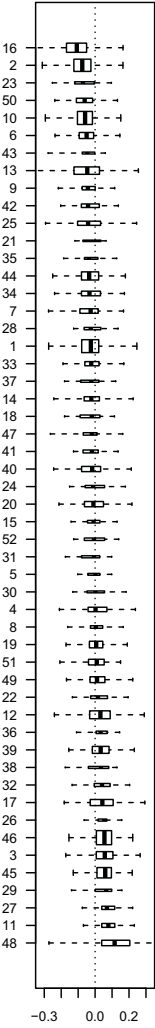
**Hippocampus AI against ICV**



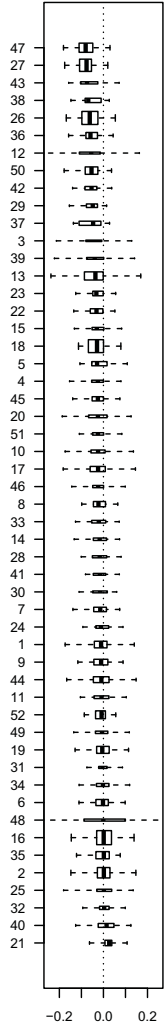
### **Supplementary Information S6.**

Boxplots of AI distributions for each dataset and structure. For each structure, the datasets are ordered top-to-bottom by their median AIs. The identities of the datasets are given by the numbers in the lefthand columns, with reference to Table 1. The horizontal length of each box represents the 2nd to 3rd quartile of the AI distribution (i.e. containing half of subjects in each dataset) and split at the median AI. The vertical width of each dataset's box is proportional to the square root of its sample size. The whiskers show the minimum and maximum values (curtailed in cases where the outer box boundary was reached). The vertical dotted lines indicate the points of perfect symmetry,  $AI=0$ .

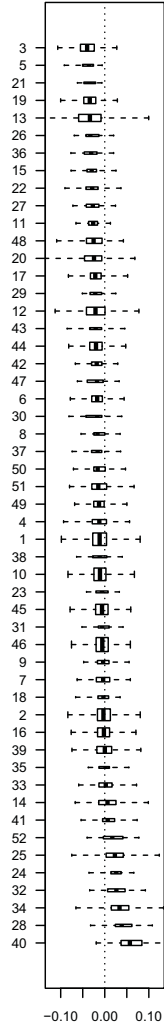
**N. accumbens**



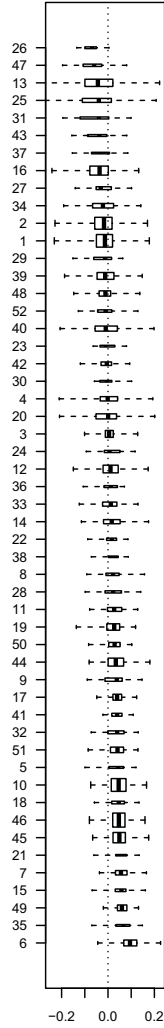
**Amygdala**



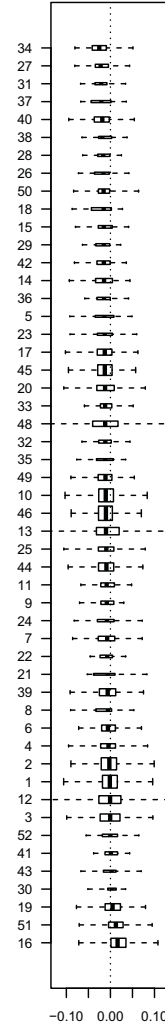
**Caudate N.**



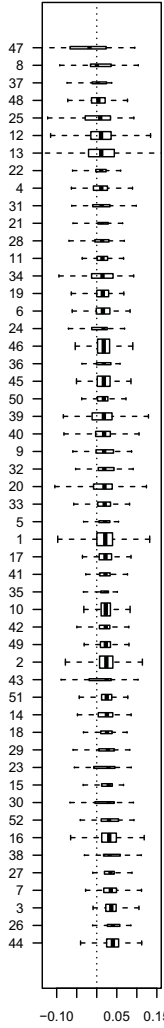
**Globus pallidus**



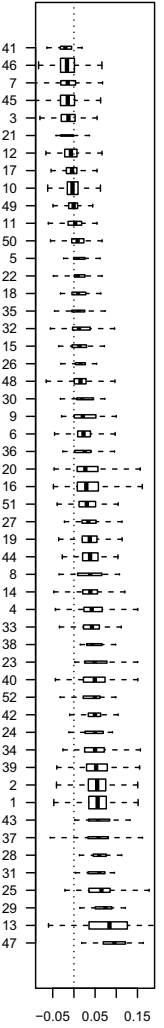
**Hippocampus**



**Putamen**



**Thalamus**



Supporting Information S7. Meta-analyzed results from testing population-level lateralization (mean AI's  $\neq 0$ ) separately by sex. A positive Z-score indicates leftward asymmetry in volume (L>R), while a negative Z-score reflects a rightward asymmetry (R>L).

Females	N	z-score	Males	N	z-score
Nucleus accumbens	7957	-11.01	Nucleus accumbens	7053	-4.80
Amygdala	8049	-33.36	Amygdala	7118	-32.72
Caudate nucleus	7980	-34.92	Caudate nucleus	7125	-31.12
Globus pallidus	7892	23.61	Globus pallidus	7040	31.16
Hippocampus	7971	-22.67	Hippocampus	7075	-20.14
Putamen	7920	59.86	Putamen	7041	53.16
Thalamus	8043	41.43	Thalamus	7115	33.44

Phenotype 1	Phenotype 2	Phenotype correlation	Phenotype correlation P	Genetic correlation	Genetic correlation P
AI_amygdala	AI_accumbens	0.00	0.90028	-0.99	0.0126487
AI_amygdala	AI_caudate	0.10	0.0001192	0.85	0.0914741
AI_amygdala	AI_hippocampus	0.00	0.9357421	-0.81	0.0356209
AI_amygdala	AI_pallidum	0.03	0.2340173	-0.42	0.3471581
AI_amygdala	AI_putamen	0.09	0.0005557	0.13	0.716055
AI_amygdala	AI_thalamus	-0.06	0.0209367	-0.10	0.7943838
AI_caudate	AI_accumbens	-0.08	0.0040859	0.32	0.3575671
AI_caudate	AI_hippocampus	-0.03	0.3293978	-0.36	0.2211863
AI_caudate	AI_pallidum	0.05	0.0393021	-0.11	0.752416
AI_caudate	AI_putamen	0.12	4.46E-06	-0.14	0.6170061
AI_caudate	AI_thalamus	0.04	0.1032485	0.31	0.3141842
AI_hippocampus	AI_accumbens	0.00	0.9842037	-0.11	0.6521278
AI_hippocampus	AI_pallidum	0.02	0.4847126	0.10	0.6775807
AI_hippocampus	AI_putamen	0.01	0.7405954	0.04	0.8433021
AI_hippocampus	AI_thalamus	0.11	3.29E-05	0.10	0.6507085
AI_pallidum	AI_accumbens	0.07	0.0068105	0.18	0.5735795
AI_pallidum	AI_putamen	0.05	0.0446912	-0.12	0.6430572
AI_pallidum	AI_thalamus	-0.21	7.16E-16	-0.26	0.3783415
AI_putamen	AI_accumbens	-0.02	0.4199311	-0.61	0.0202141
AI_putamen	AI_thalamus	-0.26	8.26E-23	-0.48	0.0365587
AI_thalamus	AI_accumbens	-0.05	0.0873988	-0.14	0.6142865

**Supplementary Information S8.** Phenotypic and genetic correlations among AIs in the GOBS dataset.